RSC Advances

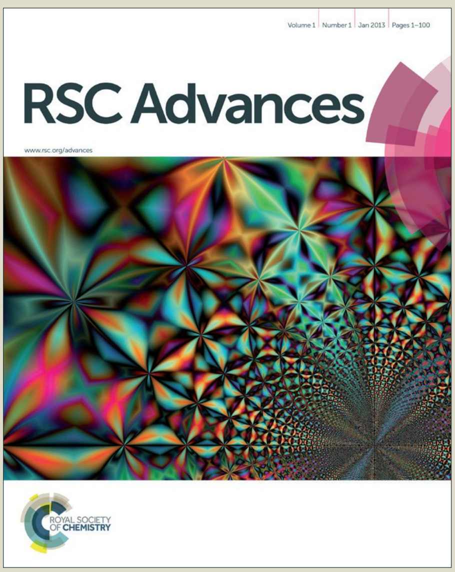

RSC Advances ARTICLE

Crystal feature and electronic structure of novel mixed alanate $LiCa(AlH_4)_3$: A density functional theory investigation

Cite this: DOI: 10.1039/x0xx00000x

Received xxth xxxxxxx 2014
Accepted xxth xxxxxxx 2014

DOI: 10.1039/x0xx00000x

www.rsc.org/

Hai-Chen Wang[a], Jie Zheng[a], Dong-Hai Wu[a], Liu-Ting Wei[a], Bi-Yu Tang[a,b,*]

The crystal structure of $LiCa(AlH_4)_3$ was investigated via first principle calculations, especially the positions of hydrogen atoms undetected in XRD experiment were predicted, then the thermodynamic favourability of experimentally reported structure with respect to several candidates from inorganic crystal structure database (ICSD) was confirmed. It is found that the hexagonal packing of AlH_4 layers along c axis is present in $LiCa(AlH_4)_3$, and the detailed geometrical feature is further revealed. The electronic structures show that in $LiCa(AlH_4)_3$ the Li–AlH_4 interaction is more covalent than in $LiAlH_4$, while the Ca–AlH_4 covalence is less than ones in $Ca(AlH_4)_2$. The overall stronger covalence in $LiCa(AlH_4)_3$ leads to weakened Al–H bonds. The Li–H interaction in $LiCa(AlH_4)_3$ dramatically turns to be strong bonding, opposite to the Li–H anti-bonding in $LiAlH_4$. The Ca–H bonds are more anti-bonding in $LiCa(AlH_4)_3$.

Introduction

Although the use of coal and petroleum as conventional energy enabled the industrial revolution, today the world is threatened not only by the environmental pollution, but also by the depletion of fossil fuels. In the last few decades, the search for alternative energy has been gradually focused on one of the most potential candidates —hydrogen, which is sustainable and clean. However, safe and efficient hydrogen storage methods for on-board application still need developing.

Recently, lightweight hydrides, including borohydrides, amides, and alanates have been considered as promising storage materials and attract wide attentions due to their high hydrogen content.[1-4] And the important development of the analogous hydrogen storage materials has been increasingly achieved. [2-7] In 1997, Bogdanović and Schwickardi[8] found that doping with Ti makes $NaAlH_4$ dehydrogenation reversible under moderate condition. This discovery boosts a strong interest in studying catalysed alanate systems as well as searching for novel alanates with optimal thermodynamic and kinetic properties.[1,9-18] Subsequent studies show that mixing two alkali or alkaline earth metals in the alanates makes it possible to obtain mixed alanates as well as adjust the desorption temperatures,[10,19] and dozens of mixed alkali alanates (Na_2LiAlH_6 [20-29], K_2LiAlH_6 [20,21,29-31], and K_2NaAlH_6 [20,21,32]) with hydrogen desorption reversibility were observed. Furthermore, Experimental efforts [21,33] and DFT investigation [34] proved that the improved properties of the mixed alanates were attributed to the destabilization effect of the smaller alkali ions.

Recently, $LiMg(AlH_4)_3$ was found to release 7.3 wt.% H_2 below 190 ℃.[19,35-37] More recently, $LiCa(AlH_4)_3$ was obtained from ball-milling $LiAlH_4/CaCl_2$ mixture.[38] This new alanate is very attractive because it starts to desorb hydrogen around 120 ℃ and release 7.8 wt.% hydrogen below 400 ℃.[38] The space group, lattice constants, and internal coordinates of metal atoms of this novel mixed alanate were obtained by XRD measurement, but the positions of hydrogen atoms were not determined due to the low X-ray sensitivity of hydrogen atom.[38] Moreover, the possible rotation of $[AlH_4]^-$ tetrahedron would bring difficulty into the determination of hydrogen positions, as in the case of $Ca(AlH_4)_2$.[39,40] Therefore, the interactions between hydrogen and metal atoms in this attractive material remained unclear. Because fundamental knowledge of atomic structure is urgently required to further develop $LiCa(AlH_4)_3$ as practical hydrogen storage system, the details of its crystal structure need a full investigation. It has been reported that DFT calculations successfully predicted the crystal structure of several analates, *e.g.* $Ca(AlH_4)_2$ [39,40], $Mg(AlH_4)_2$ [41], K_2LiAlH_6 [20,21,30,31], and $LiMg(AlH_4)_3$ [19,35]. Therefore, on the basis of first principle calculations we investigate the crystal structure of $LiCa(AlH_4)_3$ and determine the coordinates for H atoms, then provide a clear picture of the atomic and electronic structure within this material.

Methodology

Our calculations were carried with density function theory (DFT) and plane wave basis set, as implemented in Vienna Ab initio Simulation Package (VASP).[42,43] Electron-ion interactions were treated by the projected augmented wave (PAW) method,[44] and the PW91 gradient corrected exchange-correlation functional [45] was applied. A 650 eV energy cutoff was applied in all calculations and the Brillouin zone of solid phases was sampled with 0.1 $Å^{-1}$ spacing of the k-point meshes. The Gauss broadening of 0.1 eV was applied to integrate the Brillouin zone in structure relaxations, and in static calculations the tetrahedron method with Blöchl corrections was applied. The criterion for convergence of the Hellmann–Feynman forces was 0.01 eV/Å, and the calculated total energy was converged within 0.1 meV/cell.

Results and discussion

Determination of ground state structure

The crystal structure of $LiCa(AlH_4)_3$ recently determined by XRD possesses *P*63/*m* (No. 176) symmetry, while the coordinates of H atoms are not given due to low X-ray sensitivity of hydrogen atom.[38] However, the possible Wyckoff positions of hydrogen atoms could be limited by space group symmetry. Because H atoms should form AlH_4 tetrahedrons as in other tetra-aluminates [19-21,30,31,35,39-41] and the Wyckoff position of Al is at 6h,[38] to fulfil the H/Al ratio and the symmetry of AlH_4 tetrahedrons, the reasonable Wyckoff positions for H atoms in space group *P*63/*m* should be two 6h positions lying in the same (004) plane with Al atom and one 12i position showing mirror symmetry with respect to the (004) plane, as displayed in Fig. 1. This is analogous to $CdTh(MoO_4)_3$ with the same $AB(CX_4)_3$ stoichiometry and *P*63/*m* space group, where Mo atoms are also at the same 6h site, and the O atoms occupy two 6h and one 12i sites. It is noticeable that the symmetry of space group *P*63/*m* does not rule out different orientations of AlH_4 tetrahedrons on (004) plane.

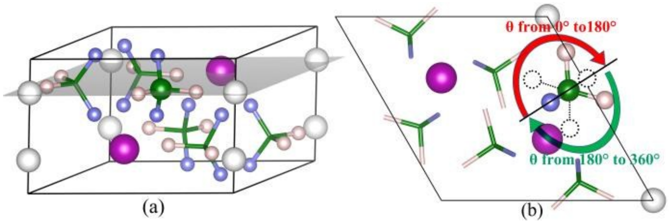

Fig. 1. Side (a) and top (b) view of $LiCa(AlH_4)_3$ crystal structure with experimentally determined space group *P*63/*m*. White, purple, and green spheres denote Li, Ca, and Mg atoms, respectively. Pink (blue) balls denote the H atoms on 6h (12i) sties. In (b), dotted circles denote the H positions after the AlH_4 tetrahedrons rotated 180° and arrows denote the rotation direction.

In order to search for possible stable orientations of AlH_4 tetrahedrons, according to the above hydrogen Wyckoff positions together with the average Al–H distance in other tetra-alanates,[19-21,30,31,35,39-41] all tetrahedrons were synchronic "rotated" under strictly limitation of the space group symmetry, here 36 images were constructed along the "rotation path" which is shown in Fig. 1(b) as red and green arrows. Then all images were adequately optimized except the fixed orientation angle θ. The variation of total energy along the rotation path was plotted as a function of θ in Fig. 2.

It can be seen that the most thermodynamically stable structure is the first image (with θ equals to zero). This starting image was considered as the initially determined structure (IDS) of $LiCa(AlH_4)_3$ crystal, which is similar to the structure of $CdTh(MoO_4)_3$. The energy profile also provides an estimate of energy barrier for the synchronic rotation of all AlH_4 complex anions. Although there are several local minimal orientations along the rotation path, the energy barriers are obviously too high for synchronic rotating all tetrahedrons under strictly limitation of the space group symmetry.

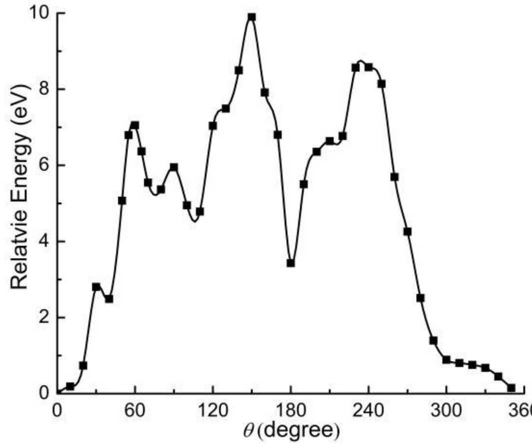

Fig. 2. The energy profiles for orientation variation of AlH_4 tetrahedrons in $LiCa(AlH_4)_3$ crystal structure within space group *P*63/*m* determined by experiment in Ref. 38.

To further confirm the thermodynamic stability of our IDS with respect to other possible $LiCa(AlH_4)_3$ candidate structures, we performed calculations of structural analogue in searching for other possible $LiCa(AlH_4)_3$ structures on the basis of the inorganic crystal structure database (ICSD). The recently reported $LiMg(AlH_4)_3$ structure is specifically taken as a template. Because seldom quaternary complex compounds with exactly ABC_3D_{12} stoichiometry are presented, several quaternary complex compounds with closely related stoichiometries are considered.[19,35] The candidate $LiCa(AlH_4)_3$ structures were created by replacing the cations (A and B atoms) in the templates with Li and Ca, then substituting Al and H for complex functional group anions. If necessary, some extra cations of several quaternary complex compounds with closely related stoichiometries were deleted to obtain the $LiCa(AlH_4)_3$ stoichiometry. To evaluate the thermodynamic stability of other possible $LiCa(AlH_4)_3$ structures, we optimized both the atomic positions and the cell vectors for all candidate structures, and the calculated total energies per formula unit relative to the most stable structure (*E*r) are listed in Table 1.

Table 1. The relative total energies (E_r, in kJ/mol per formula unit) of $LiCa(AlH_4)_3$ candidate structures.

Templates	Space group	E_r
IDS	*P*63/*m*	0
$LiMg(AlH_4)_3$	*P*21/*c*	4.9
$K_2Mg_2(SO_4)_3$	*P*213	5.2
$Al_2K_3(PO_4)_3$	*Pna*21	13.3
$Li_2V_2(PO_4)_3$	*P*21/*n*	14.9
$CeFe(WO_4)_3$	*P*-1	22.0
$Mn_4Rb(AsO_4)_3$	*Pnnm*	28.4
$Ni_2Rb_2(MoO_4)_3$	*P*21/*c*	30.6
$Li_2Mg_2(MoO_4)_3$	*Pnma*	74.3
$GdB_4(AlO_4)_3$	*R*32	76.0
$Ag_{1.5}In_{1.5}(MoO_4)_3$	*I*41	112.9

Our IDS on the basis of experimental determined information has the lowest energy comparing with other possible $LiCa(AlH_4)_3$ candidate structures. Two candidates with $LiMg(AlH_4)_3$ and cation-eliminated $K_2Mg_2(SO_4)_3$ prototypes have, respectively, the second and third lowest energies. The energy differences between these two candidates and IDS are around 5 kJ/mol per formula unit. This minor energetic difference implies that all these crystal structures may be stable at different experiment conditions. Whereas, the searching of the possible phases at different conditions is beyond the scope of this paper. Therefore, in following investigations, we would only consider the optimized IDS as the ground state of $LiCa(AlH_4)_3$.

The optimized lattice constants and atomic coordinates of the fully relaxed IDS of $LiCa(AlH_4)_3$ are shown in Table 2, together with previous reported XRD result for comparison. The calculated values of lattice constants are slightly larger than the experimental results, but the errors are close to 2%. The overestimation of lattice constant may come from the GGA functional applied in this work, and similar error is observed in AlH_3 system.[46] Additionally, the optimized lattice parameters and atomic coordinates of the ISD calculated via GGA-PBE exchange-correlation functionals [47] show negligible differences compared to the PW91 results, as shown in Table 2. So our present investigation is fairly reliable, and the coordinates of metal atoms in optimized structure are consistent with experimental results in Ref. 38, indicating that our IDS as the XRD experimentally detected structure can be reasonable.

Table 2. The calculated lattice constants (*a* and *c*, in Å) and atomic coordinates of IDS, together with experiment results for comparison.

		IDS in this work: PW91			IDS in this work: PBE			Experimental[a]				
a		9.106			9.093			*a*		8.9197(12)		
c		6.003			5.996			*c*		5.8887(7)		
		coordinates			coordinates					coordinates		
		x	*y*	*z*	*x*	*y*	*z*			*x*	*y*	*z*
Al	6h	0.300	0.900	1/4	0.300	0.900	1/4	Al	6h	0.281	0.903	1/4
Ca	2d	2/3	1/3	1/4	2/3	1/3	1/4	Ca	2d	2/3	1/3	1/4
Li	2a	0	0	1/4	0	0	1/4	Li	2a	0	0	1/4
H	6h	0.546	0.502	1/4	0.544	0.501	1/4	H		—		
	6h	0.806	0.815	1/4	0.807	0.815	1/4					
	12i	0.534	0.752	0.029	0.535	0.754	0.029					

[a]Ref. 38

.

Geometrical feature

Upon the determination of crystal structure of this novel $LiCa(AlH_4)_3$ here, geometrical feature is necessary and inevitable for further study. Naturally, the geometrical structure of $LiCa(AlH_4)_3$ has close relation with the two mono-cation analate—$Ca(AlH_4)_2$ and $LiAlH_4$. Although the space group of $LiCa(AlH_4)_3$ crystal (hexagonal *P*63/*m*) differs from that of $Ca(AlH_4)_2$ (orthorhombic *Pbca*) [39] and $LiAlH_4$ (monoclinic *P*21/*c*) [48], hexagonal packing of AlH_4 layers is existed in all three alanates, as shown in Fig. 3. Similar layered structure can also be seen in $Mg(AlH_4)_2$ and $LiMg(AlH_4)_3$.[19] It should be noticed that in $Ca(AlH_4)_2$ and $LiAlH_4$ the hexagonal packing is respectively along the *a* and *b* direction, with adjacent layer structures remaining unchanged. In $LiCa(AlH_4)_3$, the hexagonal packing is along c direction, and the two adjacent layers rotate relative to each other by 180° around *c* axis.

Note that unlike $LiAlH_4$ in which the Li cations occupy the octahedral sites, cations in $Ca(AlH_4)_2$ and $LiCa(AlH_4)_3$ fill into the triangle sites, causing significant distortion of the lattice of AlH_4 layer. From this point of view, the structure of $LiCa(AlH_4)_3$ is much closer to that of $Ca(AlH_4)_2$. In $Ca(AlH_4)_2$, Ca atoms occupy 1/4 of the triangle site. And $LiCa(AlH_4)_3$, to some extent, could be seen as a variant of $Ca(AlH_4)_2$, in which Li atoms fill into 1/9 of the empty triangle sites and 1/3 of the Ca atoms are also replaced by Li atoms.

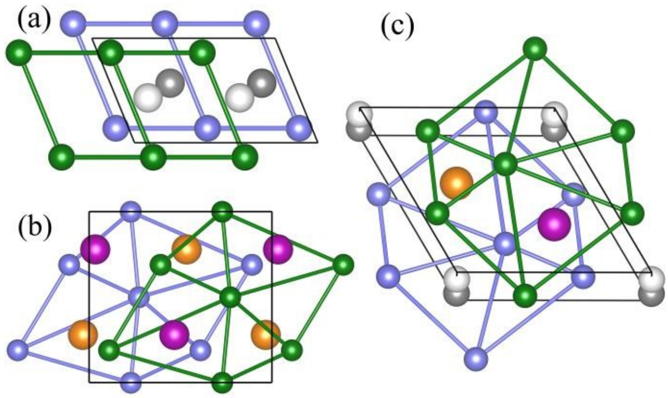

Fig. 3. Schematic diagram of the layer structure for (a) $LiAlH_4$, (b) $Ca(AlH_4)_2$, and (c) $LiCa(AlH_4)_3$ crystal viewing along *b*, *a*, and *c* axis, respectively. Green and blue spheres denote Al atoms in adjacent layers. Purple and gold balls denote Ca atoms in different layers. White spheres denote Li atoms, in (a) and (c) the Li atoms in the lower layer are represented by gray balls. H atoms are omitted for clearness.

Consequently, it can be seen from the calculated geometrical parameters in Table 3 that the in-layer distance between AlH_4 tetrahedrons d_{tetra}^{inner} in $LiCa(AlH_4)_3$ increases because of the larger number of occupied triangle sites. Although the average in-layer Al–Ca and Al–Li distances are close to that in those two mono-cation analates, the Ca–Ca bonds lying in the layer are lengthened, being consistent with the expanding layer lattice. The vertical Li–Li bonds d_{Li-Li}^{inter} in this mixed alanate are shorter and closer to the Li–Li distance in bcc-Li (2.97 Å), implying much stronger Li–Li interactions. This could be part the reason of the dramatically decreasing interlayer distance d^{inter}_{layer} in $LiCa(AlH_4)_3$. Furthermore, the coordination number of Ca increases to 9 in $LiCa(AlH_4)_3$, leading to the increasing number of Ca–H bonds around per Ca atom which serve as the inter-layer connections. Additionally, in this mixed alanate, the connection Ca–H bonds are more inclined away from c direction than ones in $Ca(AlH_4)_2$, which might also cause the decreasing interlayer distance. The average Li–H distance in $LiCa(AlH_4)_3$ significantly declines with the H coordination number of Li decreasing to 3, implying stronger Li–H interactions in this mixed alanate.

It can also be noticed from the calculated geometrical parameters in Table 3 that the AlH_4 groups slightly deviate from regular tetrahedron, this minor variations in Al-H distance and H-Al-H angles for these three materials are consistent with previous reported conclusion that the bond lengths and angles in AlH_4 tetrahedrons are almost independent to the radius of the alkali and alkaline earth cations in complex alanata hydrides.[49] Nevertheless, the very small variations of Al-H distances and H-Al-H angles within the AlH_4 anions show the order $LiAlH_4$ > $LiCa(AlH_4)_3$ > $Ca(AlH_4)_2$.

Table 3. The in-layer atomic distances (d^{inner}), interlayer atomic distances (d^{inter}), metal–hydrogen distance (d_{Al-H} and d_{Li-H}), H–Al–H bond angles (θ_{HAlH}, in degree) in $LiAlH_4$, $Ca(AlH_4)_2$, and $LiCa(AlH_4)_3$. The distances and bond lengths are in angstrom. Reference data for comparison are marked by underline.

	$LiAlH_4$			$Ca(AlH_4)_2$			$LiCa(AlH_4)_3$		
	max	average	min	max	average	min	max	average	min
d^{inner}_{tetra}	3.977	3.857 $\underline{3.869}^a$	3.736	7.042	5.166 $\underline{5.157}^b$	4.211	6.375	5.343 $\underline{5.234}^c$	3.96
d^{inner}_{Ca-Ca}		—		4.915	4.915 $\underline{4.875}^b$	4.915	6.054	6.028	6.003
d^{inner}_{Al-Li}	3.388	3.298 $\underline{3.277}^a$	3.216		—		3.288	3.288	3.288
d^{inner}_{Al-Ca}		—		3.825	3.754 $\underline{3.686}^b$	3.573	3.773	3.742	3.680
d^{inter}_{layer}		3.906 $\underline{3.901}^a$			3.362 $\underline{3.352}^b$			3.001 $\underline{2.944}^c$	
d^{inter}_{Li-Li}	3.111	3.111 $\underline{3.082}^a$	3.111		—		3.001	3.001	3.001
d^{inter}_{Ca-H}		—		2.295	2.265 $\underline{2.296}^b$	2.234	2.305	2.301	2.291
d_{Li-H}	1.989	1.909 $\underline{1.903}^a$	1.863		—		1.727	1.727	1.727
d_{Al-H}	1.645	1.627 $\underline{1.616}^a$	1.622	1.626	1.625 $\underline{1.612}^b$	1.624	1.633	1.624	1.615
θ_{HAlH}	111.0	109.5	108.4	111.4	109.5	105.5	112.4	109.4	106.7

[a]Ref. 50
[b]Ref. 51
[c]Ref. 38

Electronic Structure

Charge density. The charge density in Fig. 4(a) displays significant electron accumulation around the AlH_4 anion in $LiCa(AlH_4)_3$. Furthermore, the electron localization functions (ELF) [52] in Fig. 4(b) show strong electron localizations around H atoms, and the accumulations between Al and H atoms is weaker, being consistent with the polar covalent nature of Al–H interactions [53-55]. Additionally, the core attractors around Li and Ca cations are slightly deviated from spherical shape, and there is faint electron localization between H and Ca (Li) atoms, implying that the interactions between Ca (Li) cations and AlH_4 anios are mainly ionic and with slight covalent character.

On the basis of atoms in molecule (AIM) theory and Bader analysis,[56-59] the calculated net charge of AlH_4 anion in Table 4 for mixed alanate lies between that of two mono-cation alanates. Comparing with the situation in $LiAlH_4$, the net charge of AlH_4 anion in LiCa $(AlH_4)_3$ is less, and the electron loss from Li atoms considerably drops, indicating more covalent Li–AlH_4 interactions in the later. In comparison with $Ca(AlH_4)_2$, the net charge of AlH_4 anion in the mixed alanate is larger, and the electron transfer from Ca atoms to AlH_4 increases, implying less covalent Ca–AlH_4 ones in the mixed alanate. However, the increasing of covalency for Li–AlH_4 interaction is larger, causing the lower electron transfer from Al to H atoms within AlH_4 groups in the mixed alanate, which indicates the weakened Al–H bonds.

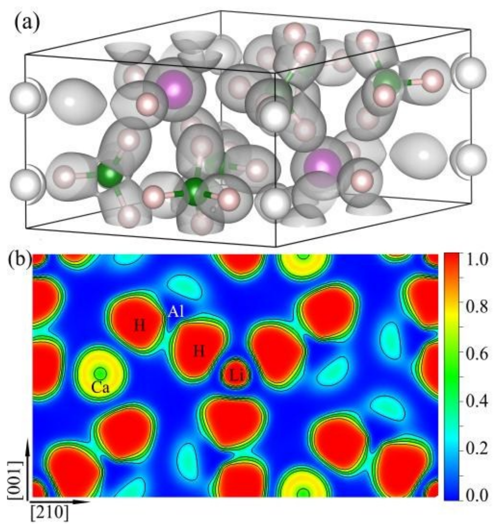

Fig. 4. (a) Side view of 3D iso-surface (with a value of 0.025 e•$Bohr^{-3}$) of total charge density for $LiCa(AlH_4)_3$. (b) Electron localization function for $LiCa(AlH_4)_3$ on (004) plane. Green, white, purple, and pink spheres denote Al, Li, Ca, and H atoms, respectively.

Table 4. The average net Bader charge in $LiAlH_4$, $Ca(AlH_4)_2$, and $LiCa(AlH_4)_3$.

	$LiAlH_4$	$Ca(AlH_4)_2$	$LiCa(AlH_4)_3$
Al	2.58	2.60	2.12
H	–0.86	–0.84	–0.72
Li	0.86	—	0.74
Ca	—	1.50	1.55
AlH_4	–0.86	–0.75	–0.76

Density of states. The density of states (DOS) of $LiCa(AlH_4)_3$ is further studied and shown in Fig. 5, together with that of $LiAlH_4$ and $Ca(AlH_4)_2$ for comparison. Obviously, all three materials could be seen as insulator.[49,60] The values of band gaps are, respectively, 4.68 and 4.67 eV, for $LiAlH_4$ and $Ca(AlH_4)_2$, being in good agreement with literature data.[39,49] The band width in $LiCa(AlH_4)_3$ slightly narrowed to 4.48 eV, implying that the excitation of electrons from the valence band into conduction band becomes easier. Thus the Al–H bonds might be easier to dissociate comparing with two mono-cation alanates.[61] In all three alanates, the valence bands have split into two parts: the lower energy ones are mainly contributed by Al–H s–s hybridization, while the Al–H p–s mixing dominates the higher energy ones. Similar to other alanates,[49] the strong Al–H hybridizations in the valence bands clearly show the covalent Al-H interaction, and the larger contribution of H-s states than that of Al s (p) states indicates the Al–H interactions are also ionic, *viz.* the Al–H bonds are polar covalent.

In $LiCa(AlH_4)_3$, the features of Al–H hybridizations resemble to that in $Ca(AlH_4)_2$, which might be caused by the similarity in their geometrical features. Careful examination shows that in $LiCa(AlH_4)_3$, H s state declines while the Al s (p) states increase within the valence band, which agrees with the weaker ionic Al–H interactions in the mixed alanate discussed above. Furthermore, comparing with $LiAlH_4$, both Al–H s–s and p–s hybridizations in $LiCa(AlH_4)_3$ shift to higher energy range, which also implies the weakened Al–H interactions in the mixed alanate. Near the Fermi level the states of cations in all three alanates overlap with Al-p and H-s states, consistent with previously reported feature that cation orbitals are hybridized mostly with the molecular orbital of AlH_4 at the highest occupied states.[62] Note that in $LiCa(AlH_4)_3$ the contribution of Li states near the Fermi level is significantly larger than in $LiAlH_4$. And the dispersion of Li states in the mixed alanate is more localized, implying that the interactions between Li and AlH_4 anions are more covalent in $LiCa(AlH_4)_3$, being consistent with the Bader charge analysis above. In contrast, the peaks of Ca states near the Fermi level are slightly lower in the mixed alanate than in calcium alanate, indicating the Ca–AlH_4 interactions are less covalent in the former.[62]
Further compared with $LiAlH_4$ and $Ca(AlH_4)_2$, more covalent Li–AlH_4 interactions and less covalent Ca–AlH_4 interactions balance each other in $LiCa(AlH_4)_3$, which makes the DOS feature of the mixed alanate lie between the two mono-cation alanates, similar to the situation in bialkili alanates.[21]

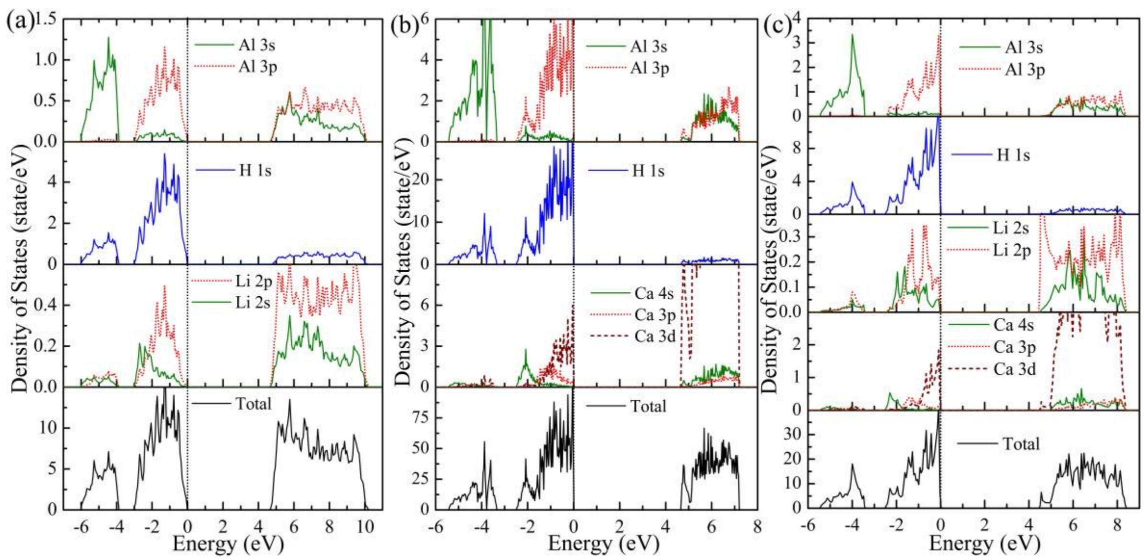

Fig. 5. The density of states of (a) $LiAlH_4$, (b) $Ca(AlH_4)_2$, and (c) $LiCa(AlH_4)_3$. The Fermi level is set at zero energy and marked by vertical dotted line.

Crystal orbital Hamilton population. To give deeper insight into the bonding character in $LiCa(AlH_4)_3$, we calculated the crystal orbital Hamilton population (COHP) via the Local Orbital Basis Suite Towards Electronic-Structure Reconstruction (LOBSTER) program,[63-65] and the results are shown in Fig. 6. The similarity of the COHP curves of Al–Ca bonds in $Ca(AlH_4)_3$ and $LiCa(AlH_4)_3$ shows analogous bonding character, being consistent with the almost unchanged inner-layer Al–Ca bond length in these two alanates as discussed above. Furthermore, the bonding character of Li–Li interactions are dramatically stronger than that in $LiAlH_4$, in accordance with the much closer Li–Li distance in $LiCa(AlH_4)_3$, which also interprets the shorter interlayer distance in $LiCa(AlH_4)_3$. Obviously, in $LiAlH_4$, $Ca(AlH_4)_2$, and $LiCa(AlH_4)_3$, bonding interaction between Al and H atoms is relatively stronger. The values of negative integrated COHP (–ICOHP) up to Fermi level for Al–H bonds are, respectively, 0.99, 0.65, and 0.60 eV/Å in $LiAlH_4$, $Ca(AlH_4)_2$, and $LiCa(AlH_4)_3$, demonstrating a decreasing sequence of Al–H bond strength. Therefore, it is reasonable to expect the Al–H bonds in $LiCa(AlH_4)_3$ are the weakest.

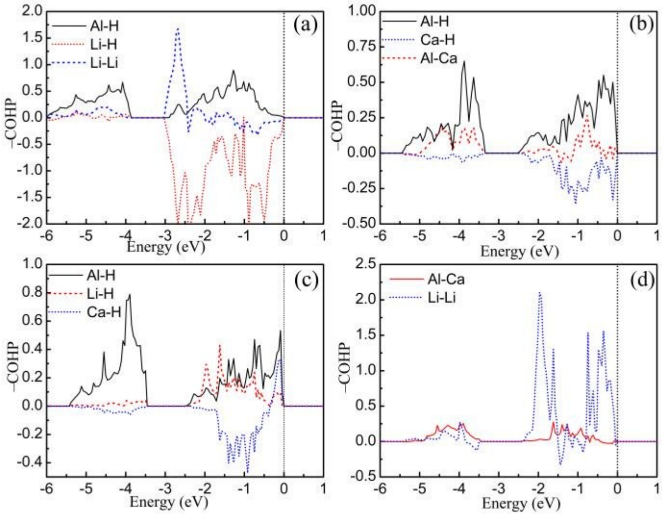

Fig. 6. The crystal orbital Hamilton population (COHP) for bonds in (a) $LiAlH_4$, (b) $Ca(AlH_4)_2$, and (c, d) $LiCa(AlH_4)_3$. The negative (positive) value of COHP indicates bonding (antibonding) contributions. The Fermi level is set at zero energy and marked by vertical dotted line.

The bonds between H and Li in $LiAlH_4$ are mostly anti-bonding, which is consistent with previous calculations.[48,49] In $LiCa(AlH_4)_3$, the Li–H interaction dramatically turns to be strong bonding, which is, to the best of our knowledge, rarely observed in alkali tetra-alanates. Considering the fact that Li–H distances in $LiCa(AlH_4)_3$ are much lower than that in $LiAlH_4$, as pointed out in discussion on crystal structure above, the Li–H orbital overlapping in $LiCa(AlH_4)_3$ might be large enough to cause bonding interactions. Moreover, the conversion from anti-bonding to bonding could also be the reason of dramatically increased covalency of Li–AlH_4 interactions,[62] which is in accordance with the more covalent Li–AlH_4 interactions in $LiCa(AlH_4)_3$ comparing with that in $LiAlH_4$. Fig. 6 also demonstrates that The Ca–H bonds in $Ca(AlH_4)_2$ are obviously anti-bonding. And the Ca–H bond becomes more anti-bonding in the mixed alanate, which agrees with the less covalent Ca–AlH_4 interactions.

Again, comparing with two mono-cation alanates, the covalent bonding features for Li–AlH_4 interactions become stronger in the mixed alanate and Ca–AlH_4 ones are more anti-bonding, which could also describe the feature of the covalence variation in cation-anion interactions as discussed above.

Conclusions

In this article, the novel mixed alanate, $LiCa(AlH_4)_3$ is investigated via DFT calculations. Based on the experimental determined hexagonal symmetry (*P*63/*m*, No. 176), hydrogen atoms positions are at first determined, and our optimized crystal structure parameters of $LiCa(AlH_4)_3$ agree well with the experimental results. The crystal structure of $LiCa(AlH_4)_3$ exhibits hexagonal packing of AlH_4 layers filled by Li and Ca within the triangle sites, similar to structure of $Ca(AlH_4)_2$ crystal. And the geometrical features are further revealed in details. The electron structures give a clear picture of the polar covalent Al–H bonds and ionic interactions between cation and AlH_4 anions. The covalency of interactions between Li(Ca) cations and AlH_4 anions in the mixed alanate lies between those of two mono-cation alanates. However, the whole covalence between Li(Ca) cations and AlH_4 anions is larger, thus the strength of Al–H bonds in $LiCa(AlH_4)_3$ are consequently weakened comparing with $LiAlH_4$ and $Ca(AlH_4)_2$. Moreover, comparison with $LiAlH_4$ and $Ca(AlH_4)_2$, hybridizations between Li and H are more localized and interaction between Ca and H in $LiCa(AlH_4)_3$ is weakened, especially the strong Li–H bonding and Ca–H anti-bonding interactions in the mixed alanate should be the main mechanism for covalency variations between Li (Ca) cations and AlH_4 anions.

Acknowledgements

The financial support from the NSFC (51461002) is gratefully appreciated.

Notes and references

[a]School of Chemistry and Chemical Engineering, Guangxi University, Nanning, 530004, China
[b]School of Material Science and Engineering, Xiangtan University, Xiangtan, Hunan Province, 411105, China
*Corresponding author:Bi-Yu Tang.Tel.: +86 731 58292195; fax: +86 731 58292468. E-mail: tangbiyu@gxu.edu.cn.

1. S. Orimo, Y. Nakamori, J. R. Eliseo, A. Züttel and C. M. Jensen, *Chem. Rev.*, 2007, **107**, 4111–4132.
2. J. Graetz and B. C. Hauback, *MRS Bull.*, 2013, **38**, 473-479.
3. B. Sakintuna, F. Lamari-Darkrim and M. Hirscher, *Int. J. Hydrogen Energy*, 2007, **32**, 1121-1140.
4. J. Graetz, *Chem. Soc. Rev.*, 2009, **38**, 73-82.
5. J. Graetz and J. J. Reilly, *Scripta Mater.*, 2007, **56**, 835-839.
6. D. Liu, C. Gao, Z. Qian, T. Si and Q. Zhang, *Int. J. Hydrogen Energy*, 2013, **38**, 3291-3296.
7. H. Cao, H. Wang, T. He, G. Wu, Z. Xiong, J. Qiu and P. Chen, *RSC Adv.*, 2014, **4**, 32555-32561.
8. B. Bogdanović and M. Schwickardi, *J. Alloys Compd.*, 1997, **253**, 1–9.
9. B. Bogdanović, U. Eberle, M. Felderhoff and F. Schüth, *Scripta Mater.*, 2007, **56**, 813–816.
10. I. P. Jain, P. Jain and A. Jain, *J. Alloys Compd.*, 2010, **503**, 303–339.
11. B. Bogdanović and G. Sandrock, *MRS Bull.*, 2002, **27**, 712–716.
12. V. P. Tarasov and G. A. Kirakosyan, *Russ. J. Inorg. Chem.*, 2008, **53**, 2048–2081.
13. B. C. Hauback, *Z. Kristallogr. Kristallgeom. Kristallphys. Kristallchem.*, 2008, **223**, 636–648.
14. A. Klaveness, P. Vajeeston, P. Ravindran, H. Fjellvåg and A. Kjekshus, *J. Alloys Compd.*, 2007, **433**, 225–232.
15. M. Ismail, Y. Zhao, X. B. Yu and S. X. Dou, *RSC Adv.*, 2011, **1**, 408-414.

16. Z. Li, F. Zhai, Q. Wan, Z. Liu, J. Shan, P. Li, A. A. Volinsky and X. Qu, *RSC Adv.*, 2014, **4**, 18989-18997.
17. J. Mao, Z. Guo and H. Liu, *RSC Adv.*, 2012, **2**, 1569-1576.
18. P. Vajeeston and H. Fjellvag, *RSC Adv.*, 2014, **4**, 22-31.
19. H. Grove, H. W. Brinks, R. H. Heyn, F. J. Wu, S. M. Opalka, X. Tang, B. L. Laube and B. C. Hauback, *J. Alloys Compd.*, 2008, **455**, 249–254.
20. O. M. Løvvik and O. Swang, *EPL*, 2004, **67**, 607–613.
21. O. M. Løvvik and O. Swang, *J. Alloys Compd.*, 2005, **404**, 757–761.
22. F. Wang, Y. Liu, M. Gao, K. Luo, H. Pan and Q. Wang, *J. Phys. Chem. C*, 2009, **113**, 7978–7984.
23. J. Huot, S. Boily, V. Güther and R. Schulz, *J. Alloys Compd.*, 1999, **283**, 304–306.
24. X. Fan, X. Xiao, L. Chen, S. Li, H. Ge and Q. Wang, *J. Mater. Sci.*, 2011, **46**, 3314–3318.
25. N. Okada, R. Genma, Y. Nishi and H.-H. Uchida, *J. Mater. Sci.*, 2004, **39**, 5503–5506.
26. J. E. Fonneløp, O. M. Løvvik, M. H. Sørby, H. W. Brinks and B. C. Hauback, *Int. J. Hydrogen Energy*, 2011, **36**, 12279–12285.
27. Y. Liu, F. Wang, Y. Cao, M. Gao and H. Pan, *Int. J. Hydrogen Energy*, 2010, **35**, 8343–8349.
28. A. Fossdal, H. W. Brinks, J. E. Fonneløp and B. C. Hauback, *J. Alloys Compd.*, 2005, **397**, 135–139.
29. J. Zhang, M.-A. Pilette, F. Cuevas, T. Charpentier, F. Mauri and M. Latroche, *J. Phys. Chem. C*, 2009, **113**, 21242–21252.
30. E. Rönnebro and E. H. Majzoub, *J. Phys. Chem. B*, 2006, **110**, 25686–25691.
31. L. Jeloaica, J. Zhang, F. Cuevas, M. Latroche and P. Raybaud, *J. Phys. Chem. C*, 2008, **112**, 18598–18607.
32. M. H. Sørby, H. W. Brinks, A. Fossdal, K. Thorshaug and B. C. Hauback, *J. Alloys Compd.*, 2006, **415**, 284–287.
33. J. Graetz, Y. Lee, J. J. Reilly, S. Park and T. Vogt, *Phys. Rev. B*, 2005, **71**, 184115-184111–184115-184117.
34. M. E. Arroyo y de Dompablo and G. Ceder, *J. Alloys Compd.*, 2004, **364**, 6–12.
35. A. R. Akbarzadeh, C. Wolverton and V. Ozolins, *Phys. Rev. B*, 2009, **79**, 184102-184101–184102-184110.
36. M. Mamatha, B. Bogdanović, M. Felderhoff, A. Pommerin, W. Schmidt, F. Schüth and C. Weidenthaler, *J. Alloys Compd.*, 2006, **407**, 78–86.
37. M. Mamatha, C. Weidenthaler, A. Pommerin, M. Felderhoff and F. Schüth, *J. Alloys Compd.*, 2006, **416**, 303–314.
38. D. M. Liu, Z. X. Qian, T. Z. Si and Q. A. Zhang, *J. Alloys Compd.*, 2012, **520**, 202–206.
39. O. M. Løvvik, *Phys. Rev. B*, 2005, **71**, 144111-144111–144111-144115.
40. C. Wolverton and V. Ozolinš, *Phys. Rev. B*, 2007, **75**, 064101-064101–064101-064115.
41. M. Fichtner, J. Engel, O. Fuhr, A. Glöss, O. Rubner and R. Ahlrichs, *Inorg. Chem.*, 2003, **42**, 7060–7066.
42. G. Kresse and J. Furthmuller, *Phys. Rev. B*, 1996, **54**, 11169-11186.
43. G. Kresse and J. Furthmuller, *Comp. Mater. Sci.*, 1996, **6**, 15–50.
44. P. E. Blöchl, *Phys. Rev. B*, 1994, **50**, 17953–17979.
45. J. P. Perdew and Y. Wang, *Phys. Rev. B*, 1992, **45**, 13244–13249.
46. C. Wolverton, V. Ozolinš and M. Asta, *Phys. Rev. B*, 2004, **69**, 144109-144101–144109-144116.
47. J. Perdew, K. Burke and M. Ernzerhof, *Phys. Rev. Lett.*, 1996, **77**, 3865-3868.
48. O. M. Løvvik, S. M. Opalka, H. W. Brinks and B. C. Hauback, *Phys. Rev. B*, 2004, **69**, 134117-134111–134117-134119.
49. O. M. Løvvik, O. Swang and S. M. Opalka, *J. Mater. Res.*, 2005, **20**, 3199–3213.
50. B. C. Hauback, H. W. Brinks and H. Fjellvåg, *J. Alloys Compd.*, 2002, **346**, 184–189.
51. T. Sato, M. H. Sørby, K. Ikeda, S. Sato, B. C. Hauback and S. Orimo, *J. Alloys Compd.*, 2009, **487**, 472–478.
52. B. Silvi and A. Savin, *Nature*, 1994, **371**, 683–686.
53. O. M. Løvvik, O. Swang and S. M. Opalka, *J. Mater. Res.*, 2011, **20**, 3199–3213.
54. A. Peles, J. A. Alford, Z. Ma, L. Yang and M. Y. Chou, *Phys. Rev. B*, 2004, **70**, 165105-165101–165105-165107.
55. V. Ozolins, E. Majzoub and T. Udovic, *J. Alloys Compd.*, 2004, **375**, 1–10.
56. W. Tang, E. Sanville and G. Henkelman, *J. Phys.: Condens. Matter*, 2009, **21**, 084204-084201–084204-084207.
57. E. Sanville, S. D. Kenny, R. Smith and G. Henkelman, *J. Comput. Chem.*, 2007, **28**, 899–908.
58. G. Henkelman, A. Arnaldsson and H. Jónsson, *Comp. Mater. Sci.*, 2006, **36**, 354–360.
59. R. F. W. Bader, *Chem. Rev.*, 1991, **91**, 893–928.
60. P. Vajeeston, P. Ravindran, A. Kjekshus and H. Fjellvåg, *J. Alloys Compd.*, 2004, **363**, L8–L12.
61. H.-C. Wang, D.-H. Wu, L.-T. Wei and B.-Y. Tang, *J. Phys. Chem. C*, 2014, **118**, 13607–13616.
62. T. Tsumuraya, T. Shishidou and T. Oguchi, *J. Phys.: Condens. Matter*, 2009, **21**, 185501 (185509 pp).
63. V. L. Deringer, A. L. Tchougréeff and R. Dronskowski, *J. Phys. Chem. A*, 2011, **115**, 5461–5466.
64. R. Dronskowski and P. E. Bloechl, *J. Phys. Chem.*, 1993, **97**, 8617–8624.
65. S. Maintz, V. L. Deringer, A. L. Tchougréeff and R. Dronskowski, *J. Comput. Chem.*, 2013, **34**, 2557–2567.

Table of Contents

Crystal feature and electronic structure of novel mixed alanate $LiCa(AlH_4)_3$: A density functional theory investigation

Hai-Chen Wang[a], Jie Zheng[a], Dong-Hai Wu[a], Liu-Ting Wei[a], Bi-Yu Tang[a,b,*]

[a]*School of Chemistry and Chemical Engineering, Guangxi University, Nanning, 530004, China*

[b]*School of Material Science and Engineering, Xiangtan University, Xiangtan, Hunan Province, 411105, China*

*Corresponding author:

Bi-Yu Tang

Tel.: +86 731 58292195; fax: +86 731 58292468.

E-mail: tangbiyu@gxu.edu.cn.

The H coordinates are predicted for $LiCa(AlH_4)_3$ in which Li–H bonding and Ca–H anti-bonding interactions are illustrated.